

Adversarial Latent Autoencoder with Self-Attention for Structural Image Synthesis

Jiajie Fan^{1,2*}, Laure Vuaille¹, Hao Wang², Thomas Bäck²

^{1*} BMW Group, Bremer Straße 6, Munich, 80788, Bavaria, Germany.

² LIACS, Leiden University, Niels Bohrweg 1, Leiden, 2333, The Netherlands.

*Corresponding author(s). E-mail(s): jiajie.fan@bmw.de;

Contributing authors: laure.va.vuaille@bmw.de;

h.wang@liacs.leidenuniv.nl; t.h.w.baeck@liacs.leidenuniv.nl;

Abstract

Generative Engineering Design approaches driven by Deep Generative Models (DGM) have been proposed to facilitate industrial engineering processes. In such processes, designs often come in the form of images, such as blueprints, engineering drawings, and CAD models depending on the level of detail. DGMs have been successfully employed for synthesis of natural images, e.g., displaying animals, human faces and landscapes. However, industrial design images are fundamentally different from natural scenes in that they contain rich structural patterns and long-range dependencies, which are challenging for convolution-based DGMs to generate. Moreover, DGM-driven generation process is typically triggered based on random noisy inputs, which outputs unpredictable samples and thus cannot perform an efficient industrial design exploration. We tackle these challenges by proposing a novel model Self-Attention Adversarial Latent Autoencoder (SA-ALAE), which allows generating feasible design images of complex engineering parts. With SA-ALAE, users can not only explore novel variants of an existing design, but also control the generation process by operating in latent space. The potential of SA-ALAE is shown by generating engineering blueprints in a real automotive design task.

Keywords: Deep generative model, Generative engineering design, Self-attention, Latent space manipulation, Structure generation

1 Introduction

Generative Engineering Design (GED) (Regenwetter, Nobari, & Ahmed, 2021; Skarka, 2007) is a novel trend of Generative Design for a more function-oriented design exploration making use of existing designs and algorithms. GED derives novel designs depending on factors such as the initial structure, desired performance and specific project requirements. As an automated exploration of industrial designs, GED shows a great potential to assist engineers in developing complex structures and speed up industrial development processes.

Deep Generative Models (DGMs) (Brock, Donahue, & Simonyan, 2018; Karras, Laine, Aittala, et al., 2019; Wu, Donahue, Balduzzi, Simonyan, & Lillicrap, 2019) seem to be a natural choice to facilitate GED, given its compelling performance in synthesizing natural images, such as landscapes, human faces, and animals. However, the implementation of DGMs as such is unlikely to bring much benefit to industrial engineering processes. One reason is that most DGMs fail to provide a controllable generation process. Recent top performing DGMs tend to use Generative Adversarial Networks (GANs) (I.J. Goodfellow et al., 2014; Radford, Metz, & Chintala, 2015) as a framework, which derives a single-generator sampling procedure and typically generates a novel image from a random noisy input. Novel models (X. Chen et al., 2016; Karras, Laine, & Aila, 2019; Mirza & Osindero, 2014) have been proposed to condition the models on additional input variables, hereby enabling fine-grained control over the generation process. These input variables are predefined attributes, such as gender, hair style or face shape in the context of human face generation. However, it is difficult to preset input conditioning variables in industrial use cases because of the lack of universal conventions used to define design parameters and large consistent labelled data. Furthermore, the relationship between the parameters and the engineering target often requires complex numerical methods to be resolved. It is thus difficult to define relevant class labels to condition the generation process. Alternatively, Adversarial Latent Autoencoder (ALAE) (Pidhorskyi, Adjeroh, & Doretto, 2020) utilizes GAN's adversarial training strategy but provides an encoder-decoder network, which allows for a mapping between image space and latent space. This architecture produces diverse images by interpreting random samples in latent space. Additionally, with sufficient analysis in the learned latent space, ALAE can be used to control the generation process by conditioning and modifying attributes in the latent space.

Another challenge lies in the fundamental difference between design images from industrial engineering processes and natural images. Natural images typically consist of textures and continuously changing color gradients, while industrial design images are defined by structural patterns, such as distinct edges, sparse shapes and their associated long-range dependencies. Most DGMs rely heavily on the convolutional operator, which excels in synthesizing realistic textures in local neighborhoods but fails to model large structural patterns (Luo, Li, Urtasun, & Zemel, 2016; Zhang, Goodfellow, Metaxas, & Odena, 2018). With convincing results, recent research (Vaswani et al., 2017; Zhang et al., 2018) demonstrates the potential of self-attention mechanism to enable DGMs to capture and model large-scale features and long-range dependencies.

To successfully adapt DGMs for engineering design applications, we propose a novel model called Self-Attention Adversarial Latent Autoencoder (SA-ALAE). We show

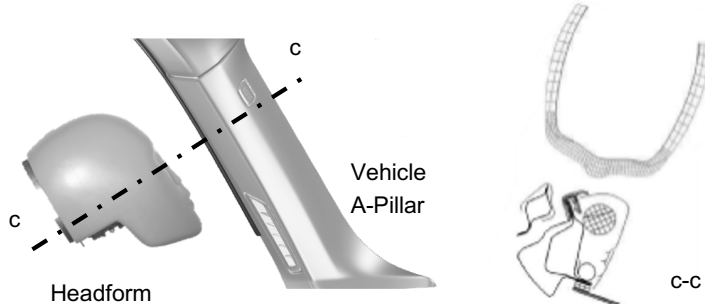


Fig. 1: Example of an automotive A-Pillar with a free motion head-form (National Highway Traffic Safety Administration, 1998)(left) and an engineering blueprint (right) obtained by extracting a cross-section from the 3D-object.

the potential of SA-ALAE by applying it in the context of automotive design exploration, where structural design is represented in engineering blueprints. To measure the quality of the synthesized blueprints, we reproduce the data-driven criteria comparison proposed by Heusel, Ramsauer, Unterthiner, Nessler, and Hochreiter (2018) based on the blueprints, and identify Fréchet inception distance (FID) as the most stable method among the criteria compared. An example of the engineering blueprint is shown in Figure 1. We further show with one experiment that SA-ALAE enables a controlled generation process by semantically modifying the encoded latent variables. The result of this experiment demonstrates the potential of SA-ALAE to understand the structural information in industrial design images, and explore novel design alternatives in desired ways. The contribution of our work is as follows:

1. We propose a novel DGM based on ALAE and the Self-Attention mechanism to enable the generation of complex structural patterns.
2. We address the need for a more reliable quantitative method than FID for evaluating the quality of synthesized engineering blueprints.
3. We propose a method to control the generative process of SA-ALAE by conditioning and modifying variables in latent space.

2 Related work

Within the domain of Deep Generative Models (DGMs), Generative Adversarial Networks (GANs) (I.J. Goodfellow et al., 2014; Radford et al., 2015) have achieved state-of-the-art performance in many image synthesis tasks (Brock et al., 2018; Wu et al., 2019). Novel models, e.g., Conditional Generative Adversarial Networks (CGANs) (Mirza & Osindero, 2014) and InfoGAN (X. Chen et al., 2016), allow users to control the generation process by adding conditional variables such as gender and face shape in the context of human-face generation. The input variables are predefined and require labeled data, which is often obtained by manual labour. In case of engineering blueprint, such classes are not available because of the complexity of

the shapes represented and also due to the lack of parameters available or conventions used to define them. However, inspired by the use of latent space to control the generation process (Bau et al., 2018; Radford et al., 2015; Shen, Gu, Tang, & Zhou, 2020), progress has been made in enabling GANs to map images to latent variables. The most successful trend is to combine GANs with encoders, which has already yielded convincing models such as BiGAN (Donahue, Krähenbühl, & Darrell, 2017), Adversarially Learned Inference (ALI) (Dumoulin et al., 2016) and Adversarial Latent Autoencoder (ALAE) (Pidhorskyi et al., 2020). These models allow an analysis of the learned latent space after training. After identification and understanding of the latent variables, semantic modification in the latent space can influence the generation process in desired ways. Among BiGAN, ALI and ALAE, the latter achieves the best image quality when tasked to reconstruct MNIST (Lecun, Bottou, Bengio, & Haffner, 1998) digits and also the highest accuracy when applying MNIST classification to its generated outputs (Pidhorskyi et al., 2020). After training, ALAE provides an encoder-decoder inference, which allows ALAE to conduct a mapping between image and latent space. Diverse designs can be produced by encoding-decoding the initial design with random noise added in the latent space.

Additionally, with sufficient analysis in the learned latent space, the ALAE can be used to condition the generated outputs by modifying only specific latent variables (Bau et al., 2018; Radford et al., 2015; Shen et al., 2020).

The architecture of ALAE is shown in Figure 2a. The ALAE implements a mapper M that generates latent variables $\omega \subset \mathbb{R}^d$ (d -dimensional) for random noise $z \sim \mathcal{N}(0, \mathcal{I})$. The space of the latent variables is indicated as \mathcal{W} . The latent variables ω serves as input to both discriminator ($D: \mathcal{W} \rightarrow \mathbb{R}$) and generator ($G: \mathcal{W} \rightarrow \mathcal{X}$), where \mathcal{X} stands for the space of data points. Each generated data point $G(\omega, \eta)$ is dependent not only on the latent variables ω but also on an optional noise η . ALAE adds an encoder ($E: \mathcal{X} \rightarrow \mathcal{W}$) to interpret the generated data $G(\omega, \eta)$ or real data x into latent variables ω , which is validated by the discriminator D to a score $D(\omega)$. ALAE can be seen as a GAN in which the pair (M, G) plays the role of the generator and the pair (E, D) that of the discriminator. ALAE utilizes an adversarial training in the data space with the optimization $\min_{M, G} \max_{E, D} V(G \circ M, D \circ E)$, where \circ is the chaining operator. Note that G and E together construct an autoencoder architecture (G, E) in the latent space \mathcal{W} , which is trained by optimizing $\min_{E, G} \Delta(\omega \parallel E(G(\omega)))$. For the inference, the pair of networks (E, G) builds up an autoencoder network in the data space, which requires a source image x and a noise $\eta \sim \mathcal{N}(0, \mathcal{I})$ as inputs and generates novel images. Additionally, feeding sampled noise z to the pair of networks (M, G) is able to generate random samples.

Since ALAE implements an adversarial training strategy like GANs, ALAE also suffers from training instability (I. Goodfellow, 2017; I.J. Goodfellow et al., 2014; Miyato, Kataoka, Koyama, & Yoshida, 2018). Many methods focus on solving this issue, e.g., zero-centered gradient penalty (Roth, Lucchi, Nowozin, & Hofmann, 2017), Spectral Normalization (Miyato et al., 2018), Batch Normalization (I.J. Goodfellow, Bengio, & Courville, 2016; Santurkar, Tsipras, Ilyas, & Madry, 2018), etc. Taking Residual Networks (ResNet) as backbone enables the training of deep architectures

without suffering from vanishing gradients and degradation in performance (He, Zhang, Ren, & Sun, 2016).

In Generative Engineering Design (GED) (W. Chen & Ahmed, 2020; W. Chen, Chiu, & Fuge, 2019; W. Chen & Fuge, 2018; Li, Zhang, & Chen, 2021), DGM has been shown its potential in synthesizing airfoil shapes from the UIUC database (University of Illinois at Urbana-Champaign, 2022), in which an airfoil shape is a single 2D curve. However, real-world engineering design images are often much more complex, as they contain multiple clear edges, sparse shapes and long-range geometric constraints. Generating such complex design images is still a challenge for convolution-only neural networks because the convolutional operator can only process information within a local neighbourhood (Luo et al., 2016; Zhang et al., 2018). Self-Attention Generative Adversarial Network (SAGAN) proposed by Zhang et al. (2018) introduces the self-attention mechanism into GANs. The implemented mechanism, Scaled Dot-Product Attention (Vaswani et al., 2017), constructs an attention map by computing the attention weights between each feature vector and the other feature vectors. This attention map presents the relationships between input features. With this attention map the model gains a global understanding of the input features and is able to efficiently capture long-range dependencies.

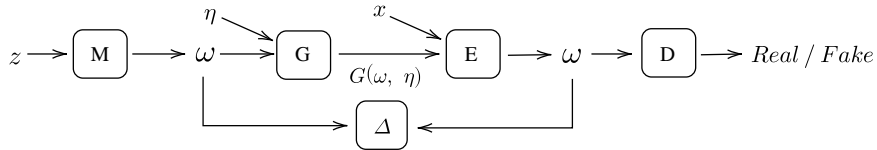
There is no universal criterion for evaluating the quality of images generated by DGMs (Salimans et al., 2016; Theis, Oord, & Bethge, 2015; Torfi, Beyki, & Fox, 2020). The most popular strategy is to measure the statistical distance between the distribution of generated images and source images, for which the Fréchet Inception Distance (FID), the Earth-Mover Distance (EMD), the Kullback-Leibler Divergence (KLD), and the Jensen-Shannon Divergence (JSD) are the most popular criteria. The performance of the criterion heavily depends on the dataset used (Theis et al., 2015). The approach proposed by Heusel et al. (2018) enables to identify a suitable criterion for a given dataset. In this approach, the distance between a source dataset and a perturbed dataset is measured repeatedly with increased level of perturbation. The suitable criterion should accurately capture the increase of perturbation.

3 Methods

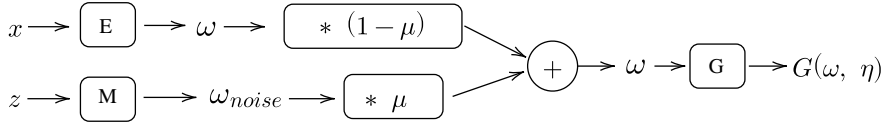
In this work, we aim at developing an appropriate DGM for enabling an efficient industrial design exploration. For this purpose, we select Adversarial Latent Autoencoder (ALAE) (Pidhorskyi et al., 2020) as a baseline framework for its flexible sampling process. We enhance the model robustness and develop an improved version by introducing modern techniques, e.g., Batch Normalization, Spectral Normalization (SN) (Miyato et al., 2018), ResNet (He et al., 2016), etc. We further implement the self-attention mechanism (Vaswani et al., 2017; Zhang et al., 2018) to enable the generation of structural patterns.

3.1 Improved ALAE

The vanilla ALAE faces a major issue in its training for the following reasons. First, the ALAE implements the adversarial training strategy in image space, which exposes it to the same training instability commonly encountered by GANs (I. Goodfellow, 2017;



(a) Training



(b) Sampling

Fig. 2: SA-ALAE architecture. ALAE and SA-ALAE share an identical training strategy. The sampling procedure of SA-ALAE utilizes the off-the-shelf mapper M to sample an additional noisy latent variables ω_{noise} , hereby introducing randomness in the sampling.

I.J. Goodfellow et al., 2014; Roth et al., 2017). The possible cause for the unstable adversarial training is that the gradients computed on the discriminator function vary too much. Besides, generating large and detailed engineering design images necessitates a deep model, which results in gradients that can easily vanish or explode. Moreover, contrary to expectations, increasing the depth of a neural network may result in a degradation of performance (He et al., 2016).

We implement the following techniques to improve the model robustness and propose a novel version of the ALAE called $ALAE_{improved}$. Firstly, to ensure that generator G receives effective gradients for the optimization, we need to prevent the computed gradients from vanishing or exploding. For this purpose, we apply Spectral Normalization (SN) (Miyato et al., 2018) in encoder E and discriminator D . Spectral Normalization is a powerful method that constrains the Lipschitz continuity of the functions optimized by E and D through layer-wise controlling the spectral norm, hereby constraining the size of the gradients. Spectral Normalization replaces every given weight matrix W by W_{sn} with the formula:

$$W_{sn} = \frac{W}{\sigma(W)}, \quad (1)$$

where $\sigma(W)$ is the greatest singular value of W . Moreover, for stabilizing the adversarial training, we implement Batch Normalization in generator G , allowing for a larger range of learning rates and to learn the data distribution more efficiently. Lastly, to address the degradation caused by increasing the depth of the neural network, we

modify generator G and encoder E of ALAE to become Residual Networks (ResNet). ResNet features in the so-called residual blocks of convolutional operators contain a “skip connection” that can bypass the error information in back-propagation, hence alleviating the vanishing gradient problem in deeper architectures.

3.2 Self-Attention Adversarial Latent Autoencoder (SA-ALAE)

Convolution-based DGMs excel in generating real-world images, i.e., sky, mountain, and lakes in landscape images. But DGMs have a hard time modeling structural objects in engineering design images. One of the main causes is that the objects in structural images can be sparsely located but are still strongly geometrically connected, e.g., in bicycle design, both wheels should be connected by an axle and lie on the ground. In this simple example, the pixels describing each wheel are depending on one another but are far away in the image. However, the convolution mechanism, as a local operator on images, cannot capture long-range dependencies, suggesting that using convolutional layers alone is unsuitable in generating engineering design images. Self-Attention Generative Adversarial Network (SAGAN)(Zhang et al., 2018) leverages the self-attention mechanism to gain a global understanding of the input features, which enables the model to efficiently capture and model long-range dependencies. Following the success of SAGAN, we introduce the same mechanism respectively into generator G and encoder E in the ALAE framework and propose a new model, Self-Attention Adversarial Latent Autoencoder (SA-ALAE).

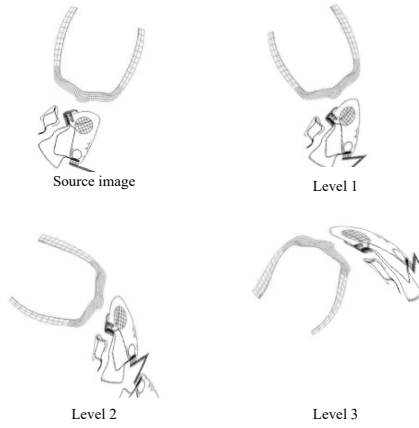
In industrial design exploration, the generation process is tasked to propose variants of an existing design. To achieve the stochastic generation of a novel image from a source image in the vanilla ALAE, the latent variables ω encoded from the original design are perturbed with sampled noise $\eta \sim \mathcal{N}(0, \mathcal{I})$. We note that this approach compromises the quality of the encoded latent variables, which leads to blurring of the generated images. To avoid this, SA-ALAE leverages the trained mapper M to sample random latent variables as noisy perturbation, which follows the learned distribution of the latent space \mathcal{W} . The novel sampling procedure of SA-ALAE is displayed in Figure 2b. Adding randomly sampled latent variables as an independent noise protects the quality of perturbed latent variables so that the stochastic encoder-decoder inference does not harm the quality of the generated image. The calculation of the latent variables, used to explore the variants of existing designs, is based on the following formula:

$$\omega = (1 - \mu) \cdot E(x) + \mu \cdot M(z), \quad (2)$$

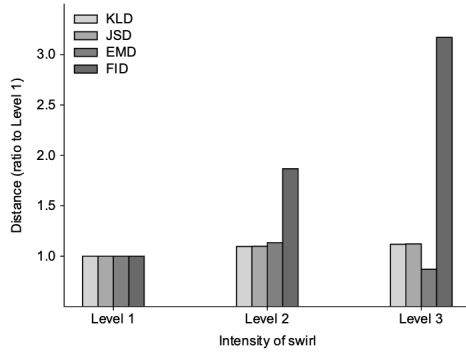
where $\mu \in [0, 1]$ is a tunable parameter, x refers to an original design and $z \sim \mathcal{N}(0, \mathcal{I})$ is sampled noise.

4 Experiments

To evaluate the performance of SA-ALAE for industrial design exploration, we trained the model to generate blueprints of vehicle parts from a real industrial design task. This dataset consists of 157 234 blueprints of various automotive structures, e.g., A-Pillars, B-Pillars, upper roof, and side rails. Extracting cross-sections from the vehicle

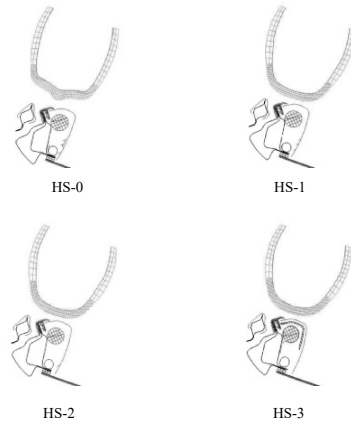


(a) Example of swirl effect on an engineering blueprint.

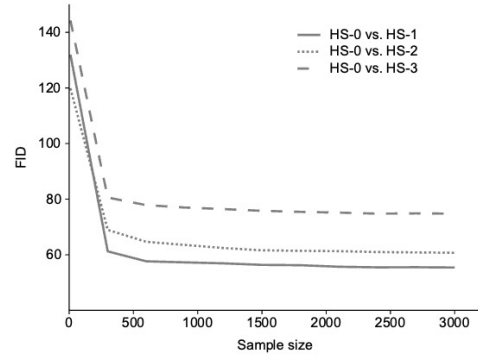


(b) Distances measured between source dataset and datasets with increased swirl perturbation.

Fig. 3: Comparison of criteria for evaluating image quality based on swirl perturbation. Three datasets are created by perturbing the source dataset with increasing levels of swirl. FID increases with the level of swirl perturbation, whereas other criteria fail to illustrate the increasing divergences brought by increasing swirl levels.



(a) Examples of blueprints from the sub-dataset APH of $Dataset_1$.



(b) Influence of sample size on FID. FIDs are measured among various cross-sections from the sub-dataset APH of $Dataset_1$.

Fig. 4: Example of vehicle A-Pillar horizontal structures and the FIDs measured in terms of sample size. The FIDs are measured between the engineering blueprints of the vehicle A-Pillar HS-0 structure and engineering blueprints of the vehicle A-Pillars HS-1,2,3 structures.

structures at various angles and locations produces different engineering blueprints, e.g., horizontal sagittal, horizontal superior, vertical sagittal, etc. In particular, for a

given vehicle structure, the horizontal-sagittal (HS-0) engineering blueprint and the horizontal-superior-1 (HS-1) engineering blueprint are produced by two parallel cross-sections close to one another and thus display a high similarity in structures. The FID measured between them are used as baseline for evaluating model performance in our work. The horizontal-superior-2 (HS-2) and horizontal-superior-3 (HS-3) engineering blueprints are also parallel cross-sections albeit taken further away in space. The sub-dataset APH consists of 12 876 blueprints of the A-Pillar structures, including HS-0, HS-1, HS-2 and HS-3 engineering blueprints. It is used as a simpler dataset to test the generative power of SA-ALAE. The blueprints are grayscale images with a resolution of 256×256 . Two different versions of this dataset are used in this study: *Dataset₁*, as some examples displayed in Figure 5a and some samples from its sub-dataset APH shown in Figure 6a; and *Dataset₂*, as some samples of its sub-dataset APH shown in Figure 7a. *Dataset₁* is an earlier database that contains irrelevant information such as a head-form model used in a specific engineering process and wire frames to fill specific areas. This additional but irrelevant information complicates the training and requires preprocessing. *Dataset₂* is a cleaner dataset, in which the head-form has been removed, images are centered on the structure and specific areas are filled with continuous grayscale color.

For the training, the initial learning rates for the optimizations $lr_{(D,E)}$, $lr_{(M,G)}$, $lr_{(G,E)}$ are respectively $1e - 4$, $2e - 4$, $1e - 4$. The batch size is 128 and the length of latent variables is set to 64. We apply a self-attention layer after each upsampling and downsampling module, where the size of the output features is 16×16 .

From each target dataset used, we randomly select 1 000 images as test data and 100 images as validation data, while the remaining images serve as training data. In accordance with the results in Section 4.1, we select Fréchet Inception Distance (FID) as the criterion to evaluate the quality of generated images during training. A higher FID indicates a larger difference between the two image datasets. In the evaluation, the model samples images for random noisy inputs, and the FID is measured between the sampled images and the corresponding source data. For computational efficiency, the FID is measured between 100 source images and 100 generated images after every epoch during the training to evaluate the model performance. If the measured FID does not improve within 20 epochs, the training procedure is terminated. The FID baseline is determined by the FID measured between neighboring cross-sections, i.e., HS-0 and HS-1 engineering blueprints taken from the sub-dataset APH of the same dataset, as one example from *Dataset₁* shown in Figure 4a. The measured FID baselines are 55.40 for *Dataset₁* and 35.58 for *Dataset₂*.

In this work, we implement various strategies to train the models:

- ALAE (Pidhorskyi et al., 2020): vanilla ALAE model trained with *Dataset₁*;
- ALAE_{improved}: improved version of ALAE, trained with *Dataset₁*
- SA-ALAE_{whole}: introducing self-attention layers into ALAE_{improved} model, trained with *Dataset₁*;
- SA-ALAE_{aph}: initial SA-ALAE model trained with the sub-dataset APH of *Dataset₁*;
- SA-ALAE_{retrain}: fine-tuning the trained SA-ALAE_{whole} model on the sub-dataset APH of *Dataset₁*;

- SA-ALAE_{iaph}: initial SA-ALAE model trained with the sub-dataset APH of *Dataset*₂.

4.1 Evaluation methods

A quantitative assessment is needed to evaluate model performance. Typically, a statistical distance between generated image set and source image set is implemented. The adequacy of the commonly used evaluation criteria, e.g., Fréchet Inception Distance (FID), Earth-Mover Distance (EMD), Kullback-Leibler Divergence (KLD), and Jensen-Shannon Divergence (JSD), depends on the source dataset. Therefore, we reproduce the comparison proposed by Heusel et al. (2018) to identify the most appropriate criterion when applied to our engineering design images.

For the comparison, we create new image sets by adding various disturbances, i.e., Gaussian noise, blur, white blocks, and swirl effect, of increasing intensity to the source images. A good criterion should detect the increasing intensity of added disturbances. Adding swirl effect transforms parts of the image as a spiral, as an example of swirl effect shown in Figure 3a. The larger the intensity level is, the more the swirl effect perturbs the source images. The relationship between the measured distance and the intensity level of swirl effect is shown in Figure 3b. FID shows the most stable performance for all types of disturbances added.

As a rule of thumb, FID is calculated with 50 000 generated samples to evaluate the performance of a trained model (Heusel et al., 2018). However, generating images of this high number incurs significant computational costs. As shown in Figure 4b, the measured FID values are very sensitive to the sample size until 1 000, where we observe a plateau. Based on this observation, it is safe to take a smaller set of 1 000 images for empirical assessment of our dataset.

We also evaluate the model performance with qualitative analysis, i.e., we assess the visual quality of the generated images in terms of blurriness, detailed structure and readability.

4.2 Quantitative Analysis

The quantitative performance measured with FID of ALAE, ALAE_{improved}, and SA-ALAE_{whole} are listed in Table 1. The FIDs measured of SA-ALAE_{iaph}, SA-ALAE_{retain} and SA-ALAE_{iaph} are shown in Table 2. ALAE_{improved} significantly reduces the FID by 52% compared to the vanilla ALAE model, while SA-ALAE_{whole} shows a further improvement over ALAE_{improved}, with a 34% decrease in FID. However, SA-ALAE_{whole} performs significantly worse than the baseline with 62% larger in terms of FID. Training an initial SA-ALAE on the sub-dataset APH from scratch improves the performance by 23% but is still outperformed by 25% by the baseline. Notably, fine-tuning SA-ALAE_{whole} on the sub-dataset APH leads to an improvement of the performance by 12% compared to the baseline. When using *Dataset*₂ as the source, SA-ALAE_{iaph} trained on the sub-dataset APH from scratch is able to overperform the baseline by 15% in terms of FID.

Table 1: FID scores. Performance of ALAE, ALAE_{improved} and SA-ALAE trained with *Dataset*₁.

Objective	FID
ALAE (Pidhorskyi et al., 2020)	284.01
ALAE _{improved}	135.52
SA-ALAE _{whole}	90.09

Bold numbers indicate the best results in this experiment

Table 2: FID scores. Performance of SA-ALAE trained with various image sets.

Objective	FID
Using <i>Dataset</i>₁ as source	
Baseline	55.40
SA-ALAE _{whole}	90.09
SA-ALAE _{aph}	69.24
SA-ALAE _{retrain}	48.78
Using <i>Dataset</i>₂ as source	
Baseline	35.58
SA-ALAE _{iaph}	30.10

Bold numbers indicate the best results in this experiment

4.3 Qualitative Analysis

For the models trained on *Dataset*₁, some generated engineering blueprints are shown in Figure 5. The synthesized images from SA-ALAE_{retrain} and SA-ALAE_{aph} are shown in Figure 6. The blueprints generated by SA-ALAE_{iaph}, a further implementation of an initial SA-ALAE model trained on *Dataset*₂, are shown in Figure 7.

Samples generated by vanilla ALAE are not always corresponding to the input blueprints in terms of structure, and the images exhibit a substantial level of blurriness such that the edges and shapes can be completely unrecognizable. After enhancing the training stability, ALAE_{improved} significantly reduces the blurriness of the generated structures, but the geometrical objects remain unrecognizable. SA-ALAE_{whole} provides more detailed blueprints and empirically validates the benefits of the self-attention mechanism. Fine-tuning SA-ALAE_{whole} on the sub-dataset APH, SA-ALAE_{retrain} is able to generate high-quality images, which however are not yet sufficiently recognizable to engineers. SA-ALAE_{aph}, trained on the sub-dataset APH from scratch shows a more stable performance and its generated images are of a higher visual quality than those from SA-ALAE_{retrain}. SA-ALAE_{iaph}, trained on *Dataset*₂, excels in generating high-quality blueprints that not only correspond to the input designs but also contain recognizable structural details.

4.4 Interpolation in Latent Space

After training, SA-ALAE can generate novel design alternatives based on a given blueprint. However, it would be useful to guide the generation process and influence the

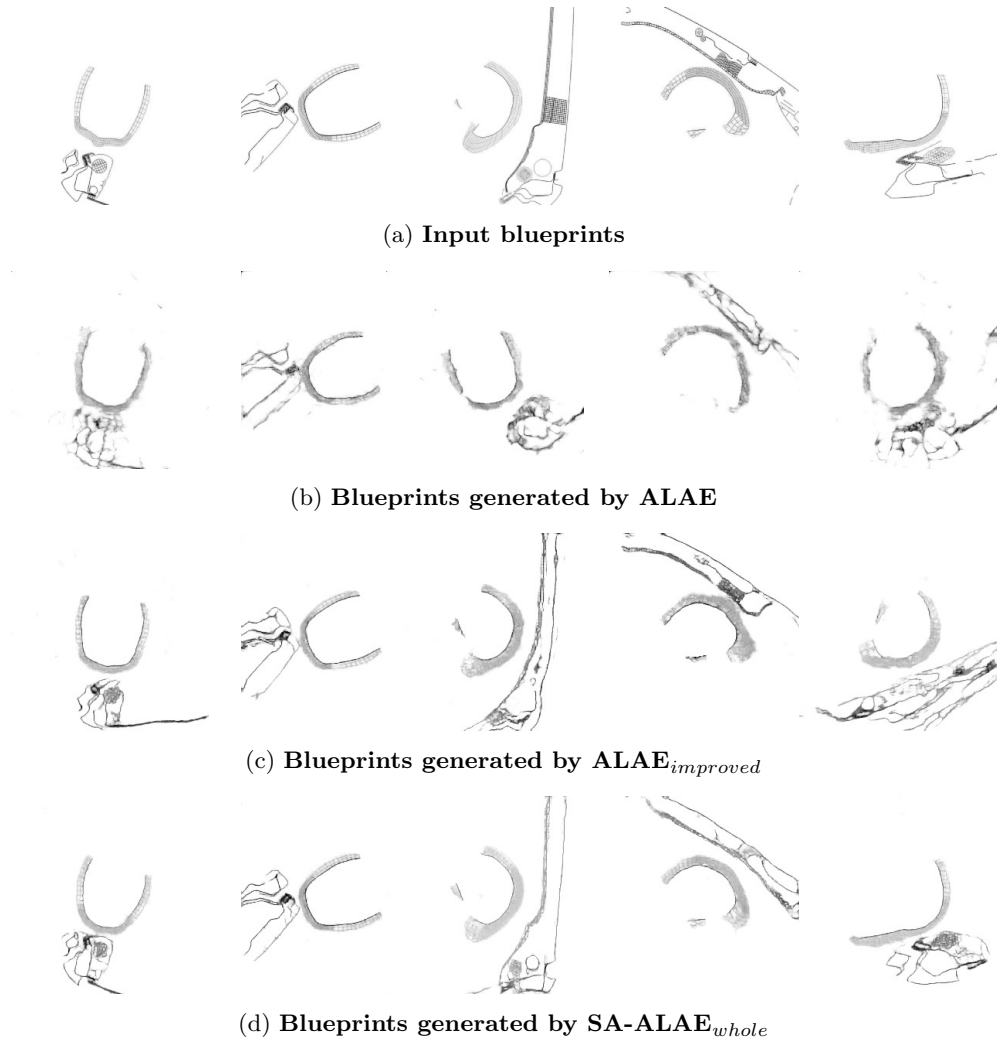


Fig. 5: Examples of source blueprints from $Dataset_1$ and blueprints generated by ALAE and SA-ALAE_{whole}

generated outputs. We hypothesize that this is made possible by the learned semantic relationship between the latent space and the patterns represented in the images. We identify two source images in which a similar object is rotated in the second image compared to the first. We show that various linear combinations of the latent variables used as input for the generator G of SA-ALAE produce novel structures with various degrees of rotation, as shown in Figure 8. The linear interpolation (Karras, Aila, Laine, & Lehtinen, 2018; Karras, Laine, & Aila, 2019) between the latent variables encoded

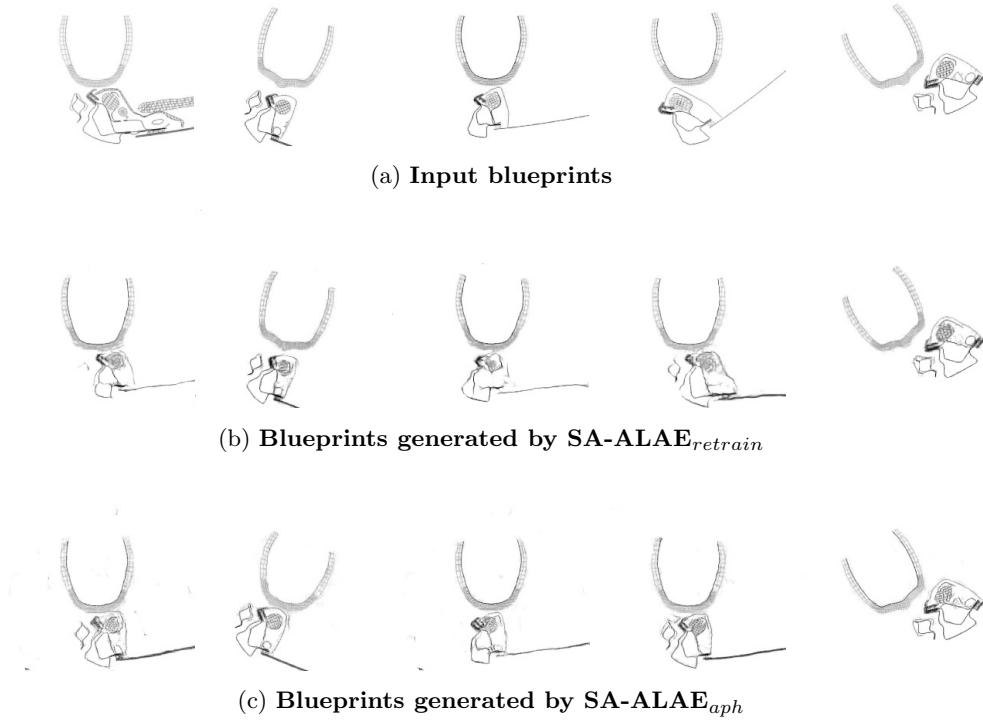


Fig. 6: Examples of source blueprints from sub-dataset APH of *Dataset*₁ and blueprints generated by SA-ALAE

from two source images is obtained by the formula:

$$\omega_{interpolated} = (1 - \alpha) \cdot \omega_1 + \alpha \cdot \omega_2, \quad (3)$$

in which α is a variable, ranging from 0 to 1, and ω_1, ω_2 are the encoded latent variables.

4.5 Discussion

ALAE provides a flexible generation process and is shown in the literature (Pidhorskyi et al., 2020) to have a GAN-like generative power on natural images. However, instead of recognizable structures, the vanilla ALAE on the vehicle A-Pillar blueprints yields only vague structures. After enhancing the model with ResNet, weight normalization, and self-attention mechanism, our SA-ALAE achieves a better FID score, and more importantly, it is able to achieve a higher image quality under expert visual inspections of the generated images. When trained with blueprints from one single structure, e.g., vehicle A-Pillars, our SA-ALAE generates blueprints that are recognizable to



(a) Input blueprints



(b) Blueprints generated by SA-ALAE_{iaph}

Fig. 7: Examples of source blueprints from sub-dataset APH from *Dataset₂* and blueprints generated by SA-ALAE_{iaph}

source 1 $\alpha = 0$	$\alpha = 0.2$	$\alpha = 0.4$	$\alpha = 0.6$	$\alpha = 0.8$	source 2 $\alpha = 1.0$
					

Fig. 8: Example of interpolation in latent space. The interpolation is conditioned on α , which is a variable ranging from 0 to 1.

engineers. However, when trained on blueprints with higher variability, i.e., structures from various vehicle components instead of A-Pillar alone, SA-ALAE demonstrates an uneven performance. An interpolation in the learned latent space shows that SA-ALAE is able to guide and control the generation process by modifying latent variables. Yet, since the components comprising a structural design are highly complex, making modifications to latent variables requires substantial effort in analyzing the learned latent space. Lastly, our selected evaluation criterion FID shows a reliable performance in distinguishing poor-quality blueprints. However, we notice that images generated by SA-ALAE_{aph} demonstrate a higher visual quality than those from SA-ALAE_{retrain}, but ALAE_{retrain} achieves a better FID score. This observation indicates that the FID

may not serve as a reliable evaluation criterion when the quality of generated images reaches a certain threshold.

5 Conclusion

In this paper, we focus on a Deep Generative Models (DGMs)-driven industrial application, which leverages existing designs and algorithms to enable automated exploration of engineering designs. We select Adversarial Latent Autoencoder (ALAE) as the base model and extend the capability of the Adversarial Latent Autoencoder (ALAE) by modifying the ALAE model with the ResNet architecture and implementing several weight regularization methods for stabilizing the training. In order to enable the generation of feasible engineering design images, we introduce the self-attention mechanism into the improved ALAE model, resulting in a novel DGM, Self-Attention Adversarial Latent Autoencoder (SA-ALAE). In contrast to the previous work in DGM-driven shape synthesis, SA-ALAE performs an image-to-image generation and is able to generate high-quality engineering blueprints of complex structures. An interpolation experiment conducted in the latent space demonstrates that the latent variables accurately represent structural information. Furthermore, modifying the encoded latent variables leads to corresponding semantic modifications in the generated structures. Despite the advances, several issues hinder an efficient application of SA-ALAE in Generative Engineering Design: (1) the current capability of SA-ALAE is insufficient for exploring designs for multiple vehicle components with a single model; (2) structural manipulation by modifying the latent space necessitates significant effort to analyze the learned latent variables and the structural attributes they represent.

Declarations

- Authors' contributions JF conceived and designed the study, conducted the research, analyzed the data, and wrote the manuscript. LV, HW, and TB supervised the research, provided guidance and expertise, and critically reviewed and edited the manuscript. All authors read and approved the final manuscript.
- Funding This work is supported by BMW Group.
- Availability of data and materials Not Applicable.
- Code availability Not Applicable.
- Conflict of interest The authors have no relevant financial or non-financial interests to disclose.
- Ethics approval Not Applicable.
- Consent to participate Not Applicable.
- Consent for publication Not Applicable.

References

- Bau, D., Zhu, J.-Y., Strobel, H., Zhou, B., Tenenbaum, J.B., Freeman, W.T., Torralba, A. (2018). *Gan dissection: Visualizing and understanding generative adversarial networks*. arXiv. Retrieved from <https://arxiv.org/abs/1811.10597>

- Brock, A., Donahue, J., Simonyan, K. (2018). *Large scale gan training for high fidelity natural image synthesis*. arXiv. Retrieved from <https://arxiv.org/abs/1809.11096>
- Chen, W., & Ahmed, F. (2020, 11). Padgan: Learning to generate high-quality novel designs. *Journal of Mechanical Design*, *143*, 031703, <https://doi.org/10.1115/1.4048626>
- Chen, W., Chiu, K., Fuge, M. (2019). Aerodynamic design optimization and shape exploration using generative adversarial networks. *Aiaa scitech 2019 forum* (p. 2351).
- Chen, W., & Fuge, M. (2018). *Béziorgan: Automatic generation of smooth curves from interpretable low-dimensional parameters*. arXiv. Retrieved from <https://arxiv.org/abs/1808.08871>
- Chen, X., Duan, Y., Houthoofd, R., Schulman, J., Sutskever, I., Abbeel, P. (2016). Info-gan: Interpretable representation learning by information maximizing generative adversarial nets. *arXiv preprint arXiv:1606.03657*, ,
- Donahue, J., Krähenbühl, P., Darrell, T. (2017). *Adversarial feature learning*.
- Dumoulin, V., Belghazi, I., Poole, B., Mastropietro, O., Lamb, A., Arjovsky, M., Courville, A. (2016). *Adversarially learned inference*. arXiv. Retrieved from <https://arxiv.org/abs/1606.00704>
- Goodfellow, I. (2017). *Nips 2016 tutorial: Generative adversarial networks*. arXiv. Retrieved from <https://arxiv.org/abs/1701.00160>
- Goodfellow, I.J., Bengio, Y., Courville, A. (2016). *Deep learning*. Cambridge, MA, USA: MIT Press. (<http://www.deeplearningbook.org>)
- Goodfellow, I.J., Pouget-Abadie, J., Mirza, M., Xu, B., Warde-Farley, D., Ozair, S., ... Bengio, Y. (2014). *Generative adversarial networks*. arXiv. Retrieved from <https://arxiv.org/abs/1406.2661>
- He, K., Zhang, X., Ren, S., Sun, J. (2016). Deep residual learning for image recognition. *2016 IEEE conference on computer vision and pattern recognition (cvpr)* (p. 770-778).
- Heusel, M., Ramsauer, H., Unterthiner, T., Nessler, B., Hochreiter, S. (2018). Gans trained by a two time-scale update rule converge to a local nash equilibrium. *Advances in Neural Information Processing Systems 30 (NIPS 2017)*, , arXiv:1706.08500 [cs.LG]

- Karras, T., Aila, T., Laine, S., Lehtinen, J. (2018). *Progressive growing of gans for improved quality, stability, and variation*.
- Karras, T., Laine, S., Aila, T. (2019). A style-based generator architecture for generative adversarial networks. *Proceedings of the IEEE conference on computer vision and pattern recognition*.
- Karras, T., Laine, S., Aittala, M., Hellsten, J., Lehtinen, J., Aila, T. (2019). *Analyzing and improving the image quality of stylegan*. arXiv. Retrieved from <https://arxiv.org/abs/1912.04958>
- Lecun, Y., Bottou, L., Bengio, Y., Haffner, P. (1998, November). Gradient-based learning applied to document recognition. *Proceedings of the IEEE, 86*(11), 2278–2324, <https://doi.org/10.1109/5.726791> (Conference Name: Proceedings of the IEEE)
- Li, R., Zhang, Y., Chen, H. (2021, oct). Learning the aerodynamic design of supercritical airfoils through deep reinforcement learning. *AIAA Journal, 59*(10), 3988–4001, <https://doi.org/10.2514/1.j060189> Retrieved from <https://doi.org/10.25142F1.j060189>
- Luo, W., Li, Y., Urtasun, R., Zemel, R. (2016). Understanding the effective receptive field in deep convolutional neural networks. *Advances in neural information processing systems* (pp. 4898–4906).
- Mirza, M., & Osindero, S. (2014). Conditional generative adversarial nets. *arXiv preprint arXiv:1411.1784*, ,
- Miyato, T., Kataoka, T., Koyama, M., Yoshida, Y. (2018). *Spectral normalization for generative adversarial networks*. arXiv. Retrieved from <https://arxiv.org/abs/1802.05957>
- National Highway Traffic Safety Administration (1998). *Federal Motor Vehicle Safety Standard No. 201U*. (TP201U-01)
- Pidhorskyi, S., Adjero, D.A., Doretto, G. (2020). Adversarial latent autoencoders. *Proceedings of the IEEE/CVF conference on computer vision and pattern recognition* (pp. 14104–14113).
- Radford, A., Metz, L., Chintala, S. (2015). *Unsupervised representation learning with deep convolutional generative adversarial networks*. arXiv. Retrieved from <https://arxiv.org/abs/1511.06434>

- Regenwetter, L., Nobari, A.H., Ahmed, F. (2021). *Deep generative models in engineering design: A review*. arXiv. Retrieved from <https://arxiv.org/abs/2110.10863>
- Roth, K., Lucchi, A., Nowozin, S., Hofmann, T. (2017). *Stabilizing training of generative adversarial networks through regularization*. arXiv. Retrieved from <https://arxiv.org/abs/1705.09367>
- Salimans, T., Goodfellow, I., Zaremba, W., Cheung, V., Radford, A., Chen, X. (2016). Improved techniques for training gans. *Advances in neural information processing systems*.
- Santurkar, S., Tsipras, D., Ilyas, A., Madry, A. (2018). *How does batch normalization help optimization?* arXiv. Retrieved from <https://arxiv.org/abs/1805.11604>
- Shen, Y., Gu, J., Tang, X., Zhou, B. (2020). *Interpreting the latent space of gans for semantic face editing*.
- Skarka, W. (2007). Application of moka methodology in generative model creation using catia. *Eng. Appl. Artif. Intell.*, 20, 677-690,
- Theis, L., Oord, A.v.d., Bethge, M. (2015). *A note on the evaluation of generative models*. arXiv. Retrieved from <https://arxiv.org/abs/1511.01844>
- Torfi, A., Beyki, M., Fox, E.A. (2020). *On the evaluation of generative adversarial networks by discriminative models*.
- University of Illinois at Urbana-Champaign (2022). *UIUC Airfoil Database*. <http://m-selig.ae.illinois.edu/ads/coord.database.html>. (Accessed on 18.10.2022)
- Vaswani, A., Shazeer, N., Parmar, N., Uszkoreit, J., Jones, L., Gomez, A.N., ... Polosukhin, I. (2017). *Attention is all you need*. arXiv. Retrieved from <https://arxiv.org/abs/1706.03762>
- Wu, Y., Donahue, J., Balduzzi, D., Simonyan, K., Lillicrap, T. (2019). *Logan: Latent optimisation for generative adversarial networks*. arXiv. Retrieved from <https://arxiv.org/abs/1912.00953>
- Zhang, H., Goodfellow, I., Metaxas, D., Odena, A. (2018). *Self-attention generative adversarial networks*. arXiv. Retrieved from <https://arxiv.org/abs/1805.08318>